

# GRB Sky Distribution Puzzles

O.V. Verkhodanov<sup>a</sup> V.V. Sokolov<sup>a</sup> M.L. Khabibullina<sup>a</sup> S.V. Karpov<sup>a</sup>

Special Astrophysical Observatory of the Russian AS, Nizhnij Arkhyz 369167, Russia

Received February 25, 2010; accepted April 21, 2010.

We analyze the randomness of the sky distribution of cosmic gamma-ray bursts. These events are associated with massive galaxies, spiral or elliptical, and therefore their positions should trace the large-scale structure, which, in turn, could show up in the sky distribution of fluctuations of the cosmic microwave background (CMB). We test this hypothesis by mosaic correlation mapping of the distributions of CMB peaks and burst positions, find the distribution of these two signals to be correlated, and interpret this correlation as a possible systematic effect.

**Key words:** cosmology: cosmic microwave background — gamma-ray bursts — cosmology: observations — methods: data analysis

## 1. INTRODUCTION

The publication of comparatively large catalogs of gamma-ray bursts based on the results of the surveys performed within the framework of space missions of the Italo-Dutch BeppoSAX satellite<sup>1</sup> (Satellite per Astronomia X, and Beppo in the honor of Giuseppe Occhialini) [1], and NASA's Compton observatory, where the BATSE experiment<sup>2</sup> (Burst and Transient Source Experiment) [2] was performed, made it possible to study the properties of the space distribution of gamma-ray bursts, which, to a first approximation, are uniformly distributed in the sky.

Among recent studies concerning this subject we distinguish the analysis of the possible relation between the distribution of gamma-ray bursts from the BATSE catalog and the large-scale structure by Williams and Frey [3]. The authors analyze the effect of the local large-scale structure on the apparent positions of gamma-ray bursts in the case of weak lensing. This effect may show up for distant ( $z > 4$ ) events as an anticorrelation of the positions of gamma-ray bursts and galaxies in clusters. The authors studying gamma-ray bursts report such an anticorrelation for galaxies at  $z \sim 0.2 - 0.3$ , which they found based on the optical magnitudes and positions of galaxies measured using the APM (Automatic Plate Measuring Facility).

In another paper, Mészáros et al. [4] use various methods (the Voronoi tessellation diagrams, the

minimal spanning tree, and multifractal spectra) to analyze the distribution of the BATSE gamma-ray bursts. The above authors break the list of objects into subsamples of sources with different signal durations ( $t < 2$  s,  $2 < t < 10$  s,  $t > 10$  s) and apply the above methods to each subsample. They found the results for the first two groups to deviate from the results obtained for uniformly distributed simulated data. Based on the data obtained the authors [4] discuss the validity of the cosmological principle.

We use the BeppoSAX (781 source, the energy interval covered: 0.1–200 keV) and BATSE (2037 sources, 20 keV–2 MeV) catalogs adopted from the sites of the corresponding experiments. We subdivide each catalog into two subsamples containing short (i.e., lasting  $t < 2$  s) and long ( $t > 2$  s) events. We thus obtain four source subsamples, which we analyze separately using the same procedure. Figure 1 shows the positions of all gamma-ray bursts from the BeppoSAX and BATSE catalogs. Figure 2 shows the positions of short and long BeppoSAX and BATSE gamma-ray bursts on separate sky charts.

In this paper we analyze the statistical correlation properties of the GRB distribution on the sky with respect to the distribution of the cosmic microwave background (CMB). We proceed from the assumption that gamma-ray bursts should be associated with massive galaxies, and that the positions of these galaxies are correlated with the large-scale structure. In this case there is hope that we may find deviations in the sky distribution of CMB fluctuations in the areas where the bursts are projected. Note that the large-scale structure may show up in CMB fluc-

<sup>1</sup> <http://www.asdc.asi.it/beposax/>

<sup>2</sup> <http://www.batse.msfc.nasa.gov/batse/>

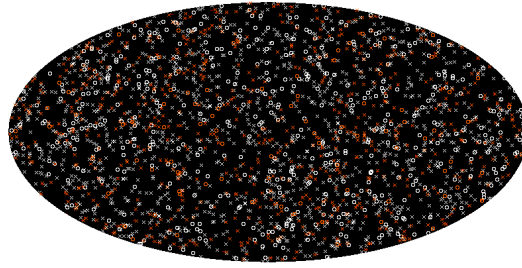


Figure 1: *Distribution of gamma-ray bursts on the sky. The gray and white symbols (the circles and crosses correspond to short and long bursts, respectively) show the BeppoSAX and BATSE data, respectively.*

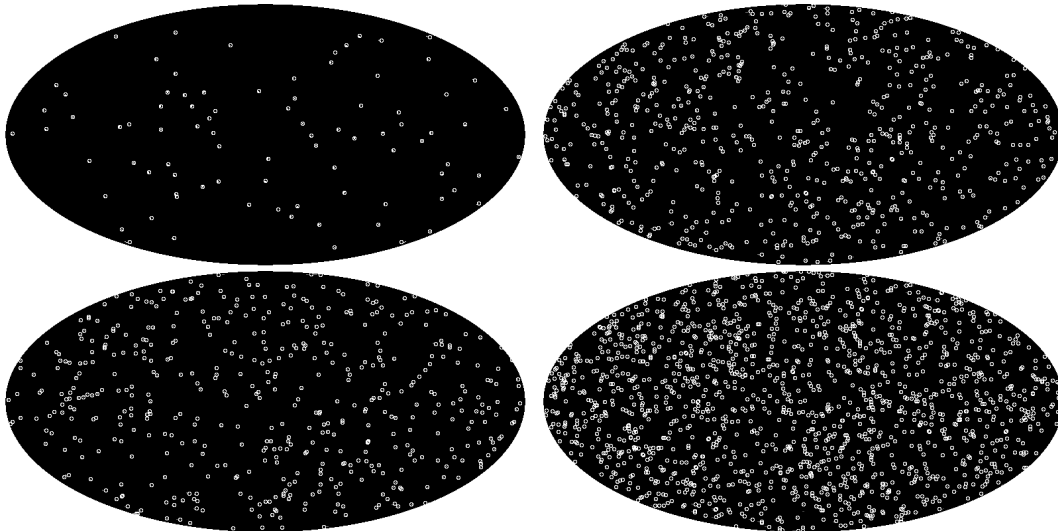


Figure 2: *Distribution of the gamma-ray bursts on the sky. The top left panel shows the BeppoSAX data for bursts with  $t < 2$  s. The top right panel shows the BeppoSAX data for bursts with  $t > 2$  s. The bottom left panel shows the BATSE data for  $t < 2$  s. The bottom right panel shows the BATSE data for  $t > 2$  s.*

tuations via the Zel'dovich–Sunyaev effect and the integrated Sachs–Wolfe effect [6]. This former effect manifests itself via the interaction of CMB photons with hot electrons of galaxy clusters [5] and is observed on the angular scales of about  $4'$  or smaller. The latter effects occurs when the photons move in a gravitational field with a variable potential that arises during the formation of the large-scale structure and expansion of the Universe, and should be observed on the angular scales greater than  $200'$ .

To study the correlation properties of the positions of gamma-ray bursts and CMB peaks, we use the CMB map based on the results of the experiment that has been conducted for seven years within the framework of the WMAP<sup>3</sup> (Wilkinson Microwave Anisotropy Probe) experiment aimed to integrate the signal from the entire sky [7]. The CMB signal was reconstructed from multifrequency observations us-

ing the method of internal linear combination (ILC) of the background components [8]. This procedure yielded the CMB map, which is also referred to as the ILC map, and which is used to analyze low-order harmonics with multipole numbers  $\ell \leq 150$ . The ILC map is based on observations made in five channels: 23 GHz (the K band), 33 GHz (the Ka band), 41 GHz (the Q band), 61 GHz (the V band), and 94 GHz (the W band).

Given that one of the central problems in statistical studies of gamma-ray bursts is due to the large error box size, about  $1^\circ \times 1^\circ$ , of the available source positions, we operate with pixels of about the same or even greater size in order to avoid uncertainties in the analysis of the sky distribution of the events.

The methods we use in this paper and our results are laid out in the following way. First we describe the methods that we use to pixelize the distribution of bursts and to correlate the maps. We then analyze the statistics of CMB deviations in the gamma-ray burst

<sup>3</sup> <http://lambda.gsfc.nasa.gov>

areas. At the next stage, we compare the BATSE–BeppoSAX and BATSE–CMB correlation maps. We finally discuss the results in the concluding section.

## 2. MOSAIC CORRELATION METHOD

To analyze the map properties on different angular scales, we expand the signal distributed on the sphere into the spherical harmonics (multipoles):

$$\Delta S(\theta, \phi) = \sum_{\ell=1}^{\infty} \sum_{m=-\ell}^{\ell} a_{\ell m} Y_{\ell m}(\theta, \phi). \quad (1)$$

Here  $\Delta S(\theta, \phi)$  are the variations of signal on the sphere in polar coordinates;  $\ell$  is the number of the multipole, and  $m$  is the number of the mode of the multipole. The spherical harmonics are determined as

$$Y_{\ell m}(\theta, \phi) = \sqrt{\frac{(2\ell+1)(\ell-m)!}{4\pi(\ell+m)!}} P_{\ell}^m(x) e^{im\phi}, \quad (2)$$

$$x = \cos \theta,$$

where  $P_{\ell}^m(x)$  are the associated Legendre polynomials. The expansion coefficients  $a_{\ell m}$  for a continuous function  $\Delta S(x, \phi)$  can be written as:

$$a_{\ell m} = \int_{-1}^1 dx \int_0^{2\pi} \Delta S(x, \phi) Y_{\ell m}^*(x, \phi) d\phi, \quad (3)$$

where  $Y_{\ell m}^*$  denotes the complex conjugate of  $Y_{\ell m}$ .

The correlation properties of two maps of the signal distribution on the sphere can be described, on a given angular scale, by a correlation coefficient for the corresponding multipole  $\ell$  as:

$$K(\ell) = \frac{\frac{1}{2} \sum_{m=-\ell}^{\ell} t_{\ell m} s_{\ell m}^* + t_{\ell m}^* s_{\ell m}}{\left( \sum_{m=-\ell}^{\ell} |t_{\ell m}|^2 \sum_{m=-\ell}^{\ell} |s_{\ell m}|^2 \right)^{1/2}}, \quad (4)$$

where  $t_{\ell m}$  and  $s_{\ell m}$  are the variations of two signals in a harmonic representation. The coefficient  $K(\ell)$  can be used to assess the correlation between the harmonics on the sphere, i.e., to compare the properties of maps on a given angular scale. However, in the case of a search for correlated areas, which do not repeat in other regions of the sphere, this approach smears such single areas in the process of averaging over the sphere within a certain harmonic. In this case it becomes practically impossible to identify the correlated areas.

Verkhodanov et al. [9] proposed an approach, which was implemented in the second release of the GLESP package [10] (the `difmap` utility). The proposed procedure makes it possible to find correlations between two maps in the areas of a certain

angular size. In this method, each pixel with number  $p$  subtending the solid angle  $\Xi_p$  is assigned the cross-correlation coefficient between the data of the two maps on the corresponding area. Thus a correlation map is constructed for two signals  $T$  and  $S$ , where the value of each pixel  $p$  ( $p = 1, 2, \dots, N_0$ , and  $N_0$  is the total number of pixels on the sphere) with the subtending angle  $\Xi_p$ , and computed for the sphere maps with the initial resolution determined by  $\ell_{max}$  is equal to

$$K(\Xi_p | \ell_{max}) = \frac{\sum_{p_{ij} \in \Xi_p} (T(\theta_i, \phi_j) - \overline{T(\Xi_p)})(S(\theta_i, \phi_j) - \overline{S(\Xi_p)})}{\sigma_{T_p} \sigma_{S_p}}. \quad (5)$$

Here  $T(\theta_i, \phi_j)$  is the value of the signal  $T$  in the pixel with the coordinates  $(\theta_i, \phi_j)$  for the initial resolution of the pixelization of the sphere;  $S(\theta_i, \phi_j)$  is the value of the other signal in the same area;  $\overline{T(\Xi_p)}$  and  $\overline{S(\Xi_p)}$  are the mean values averaged over the area  $\Xi_p$  and obtained from the data of the maps with higher resolution determined by  $\ell_{max}$ , and  $\sigma_{T_p}$  and  $\sigma_{S_p}$  are the corresponding standard deviations in the area considered.

## 3. CMB SIGNAL STATISTICS IN THE AREAS OF GAMMA-RAY BURSTS

In the first method the statistical properties of distributions of GRB positions versus the CMB signal are tested by simply analyzing the pixel value measurements on the CMB maps. We performed pixel measurements using the `mapcut` procedure of the GLESP package. Figures 3 and 4 show the positions of gamma-ray bursts of the BeppoSAX and BATSE catalog subsamples on the CMB maps with the resolution of  $260'$  ( $\ell_{max} = 20$ ) and  $36'$  ( $\ell_{max} = 150$ ). We chose the resolution of these maps to match the expected angular scale of the Sachs–Wolfe effect and the limiting resolution of the WMAP mission.

To search for the eventual correlations, we computed the number of GRB positions that fall onto the CMB pixels with negative signal fluctuations (which may be due to the effects described above) in the CMB maps of different resolution. The Table lists the statistics of CMB pixel values in the gamma-ray burst areas for the long- and short-event BATSE and BeppoSAX subsamples. It includes the total number of sources in subsamples; the number of sources located in CMB pixels with negative fluctuation values; the expected number of pixels with negative CMB amplitudes according to the results of 200 random Gaussian CMB signal simulations modeled in terms of the

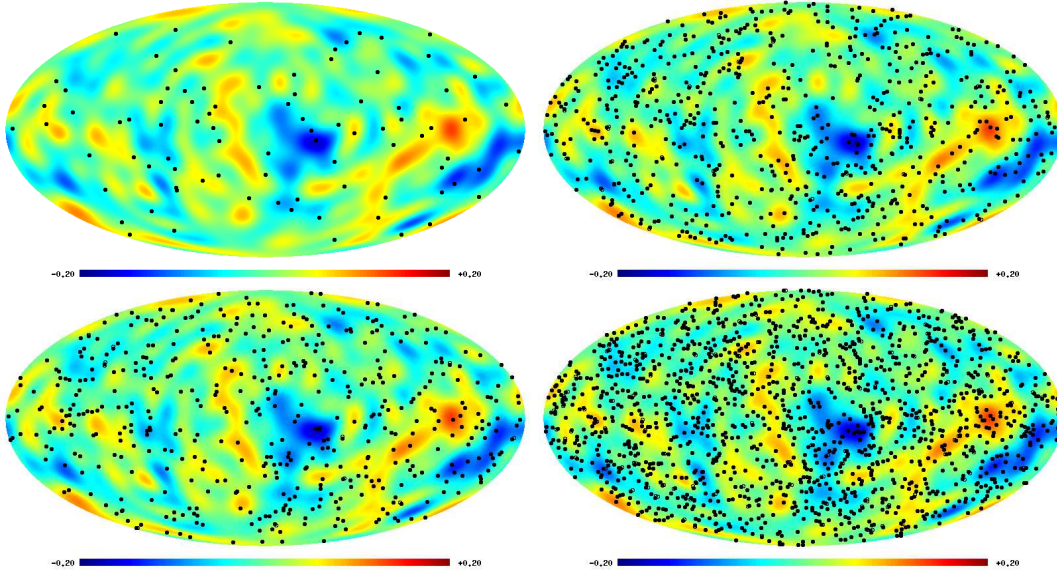


Figure 3: Positions of gamma-ray bursts from different subsamples on the CMB maps with a resolution of  $\ell_{max} = 20$ . The top left and top right panels show the BeppoSAX data for bursts with  $t < 2$  s and  $t > 2$  s, respectively. The bottom left and bottom right panels show the data for the BATSE bursts with  $t < 2$  s and  $t > 2$  s, respectively.

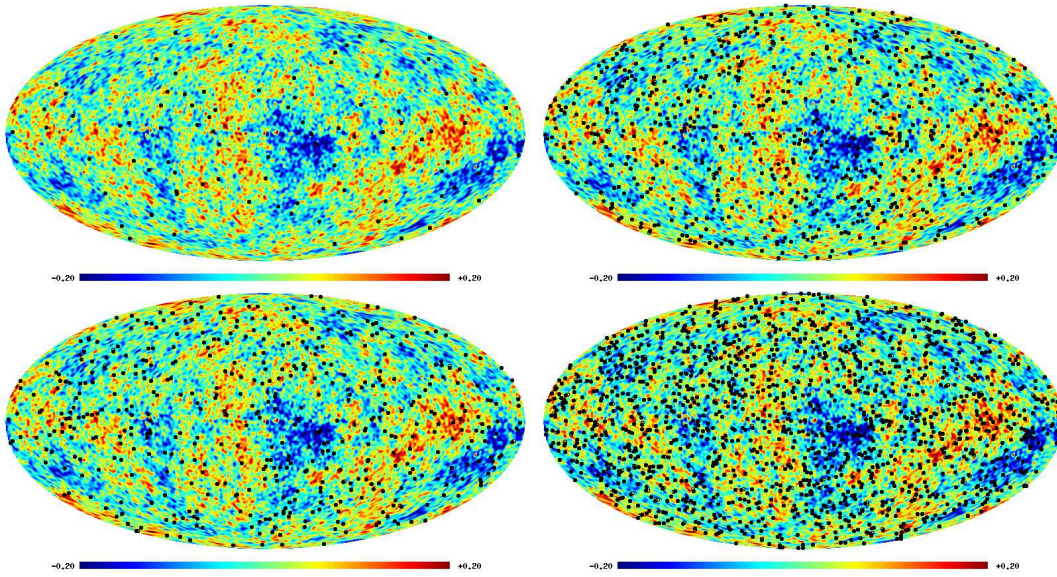


Figure 4: Positions of gamma-ray bursts from different subsamples on the CMB maps with a resolution of  $\ell_{max} = 150$ . The top left and top right panels show the BeppoSAX data for bursts with  $t < 2$  s and  $t > 2$  s, respectively. The bottom left and bottom right panels show the data for the BATSE bursts with  $t < 2$  s and  $t > 2$  s, respectively.

$\Lambda$ CDM cosmology, and the  $1\sigma$ -scatter of these quantities.

Figures 5 and 6 show the distributions of the CMB fluctuations for four gamma-ray burst subsamples and two CMB maps with different resolutions. The dashed lines show the expected  $1\sigma$  scatter of CMB

values in the  $\Lambda$ CDM cosmological model. The bottom left panel in Fig. 6, which shows the distribution of fluctuations on the CMB map with a resolution of  $\ell_{max} = 150$  in the areas of short gamma-ray bursts of the BATSE catalog, stands out conspicuously. In the positive part of the plot there is a peak, which

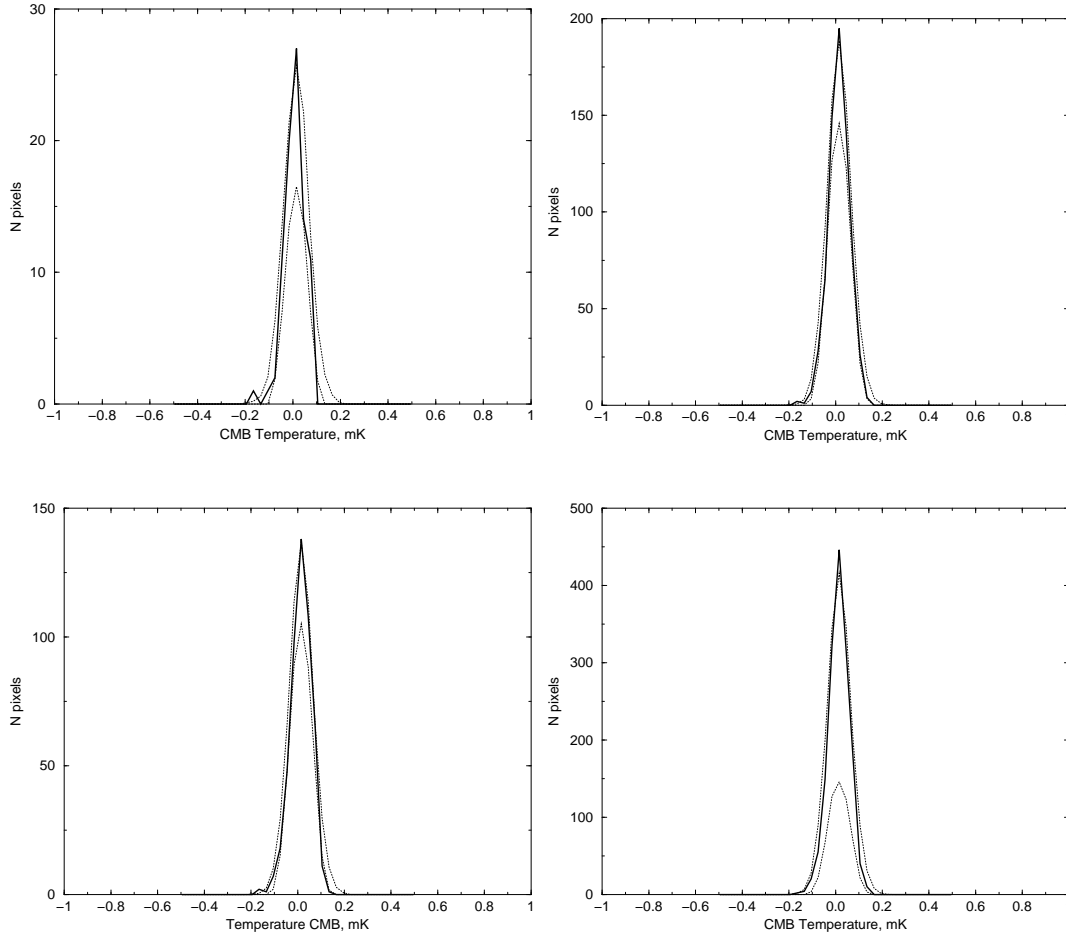


Figure 5: *Distribution of CMB fluctuations in the WMAP pixels corresponding to the GRB positions on the maps with a resolution of  $\ell_{max} = 20$ . The top left and top right panels show the BeppoSAX data for the bursts with  $t < 2$  s and  $t > 2$  s, respectively. The bottom left and bottom right panels show the data for the BATSE bursts with  $t < 2$  s and  $t > 2$  s, respectively. The dashed lines show the  $1\sigma$  scatter of CMB values in the  $\Lambda$ CDM cosmological model.*

makes the distribution deviate from Gaussianity. Figure 7 shows the positions of these bursts superimposed onto the CMB quadrupole. The statistical significance of this feature, which we estimated by generating 10000 simulated CMB realizations with the power spectrum corresponding to the  $\Lambda$ CDM model, is equal to  $7 \times 10^{-4}$ .

To analyze the distribution of GRB positions corresponding to the excess peak, we used the GLESP software package [10] to pixelize the map of burst positions. We chose the pixel size  $700' \times 700'$  in order to make the maximum pixel value (the number of events inside the corresponding area) no less than three, and to provide a significant dynamic range for the harmonic analysis. Figure 8 shows the map of selected bursts pixelized in such a way. The distribu-

tion of events on the sphere shown in the image is clearly non-uniform: it is concentrated near the ecliptic and/or equatorial poles, which is immediately apparent in the smoothed map (Fig. 9). Figure 9 also shows the ecliptic and equatorial coordinate grids, and it is evident from this figure that the asymmetry shows up both in the distribution of the signal power with respect to the equatorial plane, and in the number of spots that concentrate in the Southern Hemisphere in both coordinate systems. Note also that the hot spot above the Galactic center lies in the equatorial plane.

To reveal the asymmetries more clearly, we demonstrate a quadrupole of the smoothed map (Fig. 10) with the ecliptic and equatorial coordinate grids superimposed, as we do it in Fig. 9. It is evident

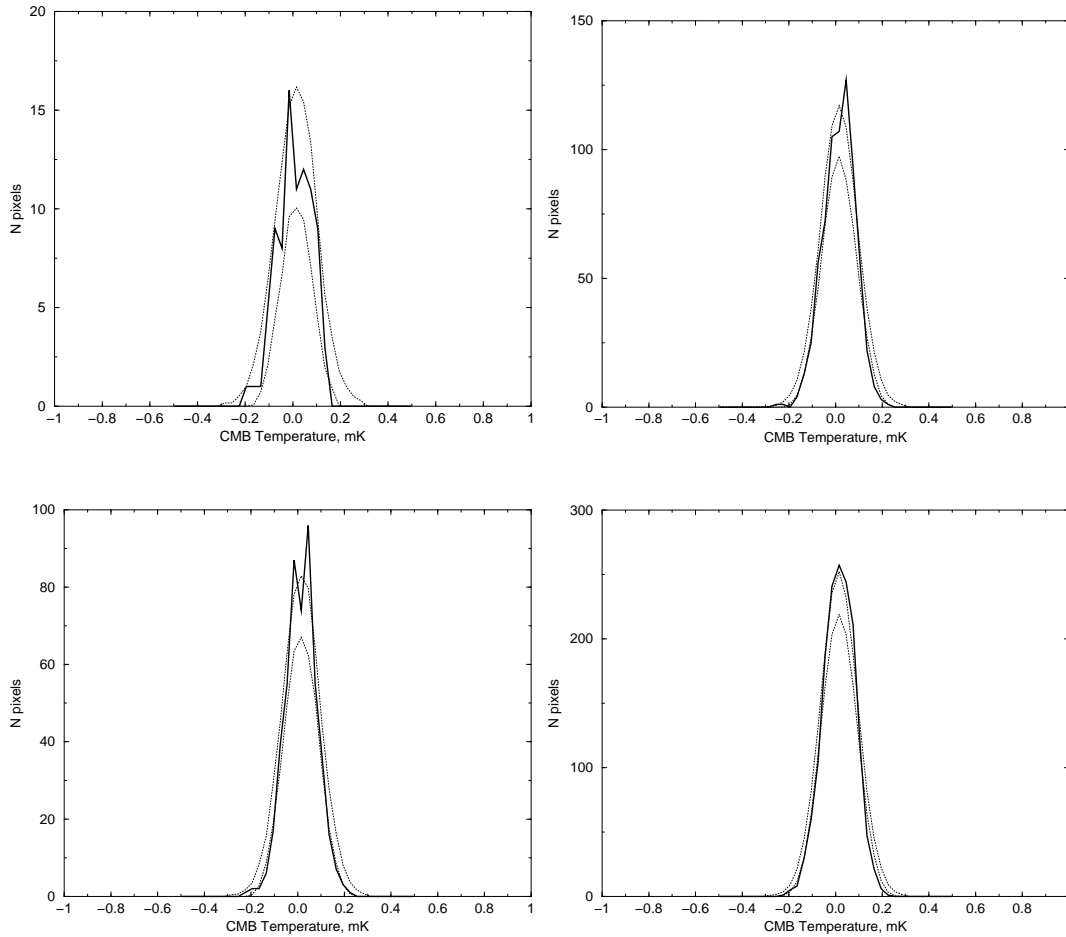


Figure 6: *Distribution of the CMB fluctuations in the WMAP pixels corresponding to GRB positions on the maps with a resolution of  $\ell_{max} = 150$ . The top left and top right panels show the BeppoSAX data for the bursts with  $t < 2$  s and  $t > 2$  s, respectively. The bottom left and bottom right panels show the data for the BATSE bursts with  $t < 2$  s and  $t > 2$  s, respectively. The dashed lines show the  $1\sigma$  scatter of CMB values in the  $\Lambda$ CDM cosmological model.*

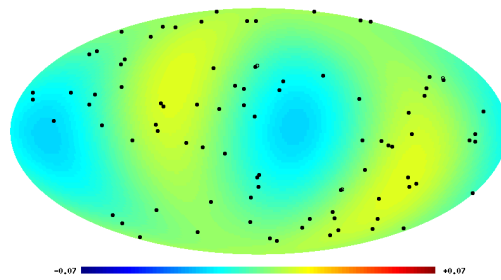


Figure 7: *Positions of short BATSE bursts corresponding to the excess in the histogram in Fig. 6 (the bottom left panel) on the map of the quadrupole ILC component.*

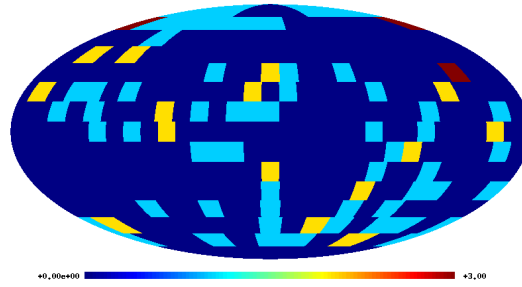


Figure 8: Pixelized map of positions of short gamma-ray bursts of the BATSE catalog corresponding to the excess in the histogram in Fig. 6 (the bottom left panel). The pixel size  $700' \times 700'$  is chosen in a way to make the maximum pixel value—the number of events inside the corresponding sky area—greater than or equal to three.

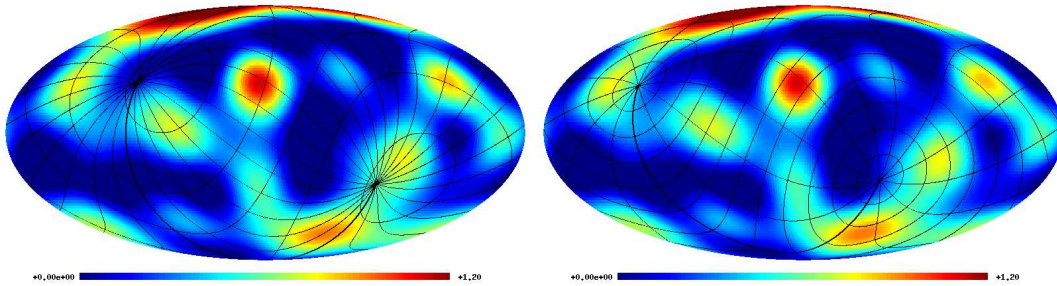


Figure 9: Smoothed sky map corresponding to the pixelization used in Fig. 8, with the ecliptic (right) and equatorial (left) coordinate grids superimposed.

Table 1: **Table.** Statistics of the CMB pixel values in the GRB areas for the BATSE and BeppoSAX subsamples. The columns are:  $t$ , the duration (s); mission name; resolution of the CMB map (the number of the multipole); total number of gamma-ray sources in the subsample ( $N_t$ ); the number of sources ( $N_e$ ) located in the CMB pixels with negative fluctuation values; expected number of pixels with negative CMB amplitudes according to the results of 200 random Gaussian CMB signal simulations, modelled in terms of the  $\Lambda$ CDM cosmology, and the  $1\sigma$ -scatter of these quantities

$t$ , s	Mission	$\ell_{max}$	$N_t$	$N_e$	Model
<2	BATSE	150	497	244	$249 \pm 11$
>2	BATSE	150	1540	763	$769 \pm 19$
<2	BATSE	20	497	250	$248 \pm 13$
>2	BATSE	20	1540	781	$768 \pm 32$
<2	BeppoSAX	150	87	43	$44 \pm 5$
>2	BeppoSAX	150	694	339	$347 \pm 15$
<2	BeppoSAX	20	87	50	$44 \pm 5$
>2	BeppoSAX	20	694	346	$348 \pm 18$

from the positions of quadrupole spots that: (1) the poles of both coordinate systems are located on the outskirts of hot spots; (2) cold spots are located sym-

metrically with respect to the equatorial planes, and (3) the Galactic center is located in the saddle-shaped area between cold and hot spots.

Our analysis of gamma-ray burst positions in the area of the peak in the distribution of short BATSE bursts with respect to the CMB revealed their unexpected sensitivity to local (near-Earth) coordinate systems. To analyze this problem in more detail, we pixelize all the four subsamples of the GRB catalogs using the method of mosaic correlation described in the previous section.

#### 4. GRB AND WMAP ILC DISTRIBUTION CORRELATION MAPS

To verify and refine the correlation properties of the maps of GRB positions and CMB fluctuations, we pixelized the maps of GRB positions for four gamma-ray burst subsamples (Fig. 11). Like at the previous stage, we chose the pixel size  $200' \times 200'$  ( $\ell_{max} = 26$ ) in order to ensure that the maximum pixel value—the number of events in the corresponding area—would be not less than three.

We then performed the mosaic correlation for the BATSE–BeppoSAX and BATSE–CMB pairs (Fig. 12). The pixel size for these correlations was

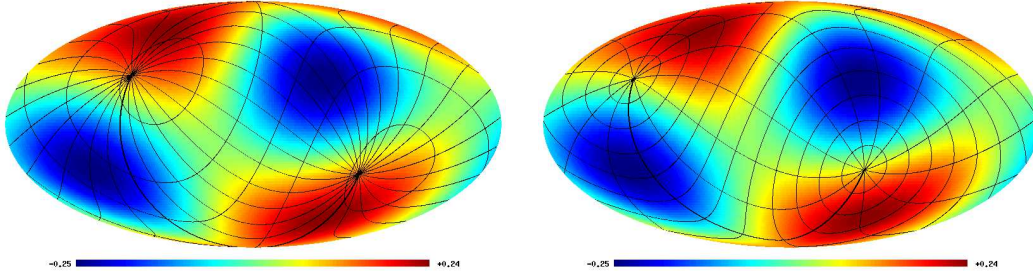


Figure 10: A quadrupole of the smoothed map (Fig. 9) with the ecliptic (right) and equatorial (left) coordinate grids superimposed.

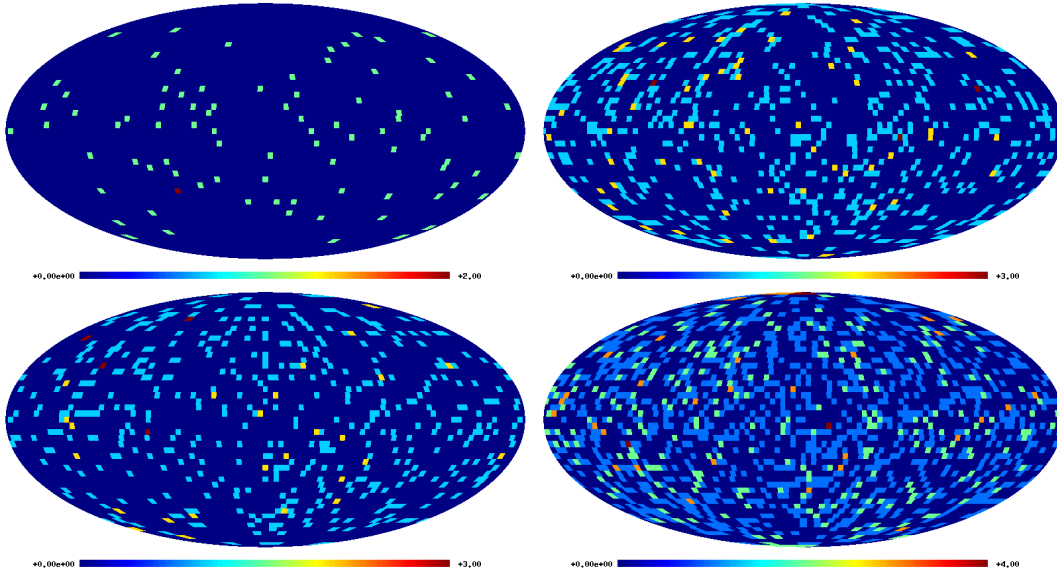


Figure 11: Pixelized maps of event positions in gamma-ray burst subsamples. The pixel size is  $200' \times 200'$ . The top left and top right panels show the BeppoSAX data for bursts with  $t < 2$  s and  $t > 2$  s, respectively. The bottom left and bottom right panels show the data for the BATSE bursts with  $t < 2$  s and  $t > 2$  s, respectively.

equal to  $500' \times 500'$ .

We can now use the expansion defined by formula (1) to compute the angular power spectrum of the map:

$$C(\ell) = \frac{1}{2\ell + 1} \left[ |a_{\ell 0}|^2 + 2 \sum_{m=1}^{\ell} |a_{\ell, m}|^2 \right]. \quad (6)$$

The power spectrum allows us to identify the main harmonics contributing to the correlation map. Figure 13 shows the power spectra of the correlation coefficient maps (mosaic correlation) between the BATSE and CMB data ( $\ell_{max} = 26$ ) and between the BATSE and BeppoSAX gamma-ray positions.

Three correlation power spectra stand out among other correlations: those between the positions of short BATSE and BeppoSAX bursts (the top left panel in Fig. 13) and between short and long BATSE

bursts and CMB fluctuations (top and bottom right panels, respectively in Fig. 13). The peaks of these spectra exhibit features that formally lie beyond the  $2\sigma$  level, and, in the case of the harmonics  $\ell = 1, 4, 7, 9$ , even beyond  $3\sigma$ . To estimate the statistical significance of these deviations, we performed numerical simulations of the zero hypothesis by generating: (1) 10,000 random realizations of the set of sky positions of the BeppoSAX gamma-ray bursts assuming that they are uniformly distributed in the sky and (2) random CMB maps with the Gaussian amplitude distribution corresponding to the  $\Lambda$ CDM cosmology, and computed the correlations and the corresponding power spectra for these simulated data in the same way as we did it for real data. Figure 14 shows the probabilities for a simulated realization to reach the deviation levels of the features observed in Fig. 13



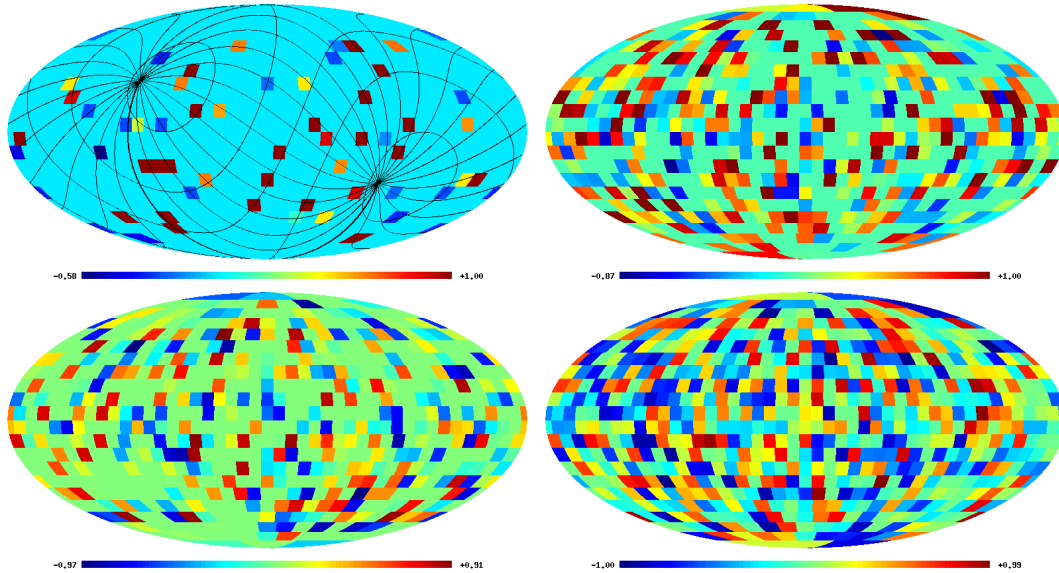


Figure 12: Correlation maps for the CMB data ( $\ell_{max} = 26$ ) and gamma-ray burst positions in the Galactic coordinate system. The pixel size for these correlations is equal to  $500' \times 500'$ . The top left panel shows the correlation between BATSE and BeppoSAX data,  $t < 2$  s, with the ecliptic coordinate grid superimposed. The top right panel shows the correlation between BATSE ( $t < 2$  s) and CMB data. The bottom left panel shows the correlation between BATSE and BeppoSAX data,  $t > 2$  s. The bottom right panel shows the correlation between BATSE ( $t > 2$  s) and CMB data.

within the framework of the zero hypothesis i.e., the significance levels of the peaks in the power spectrum. The resulting significance levels for the multipoles  $\ell = 1, 4, 7,$  and  $9$  of the correlation maps between the short BATSE and BeppoSAX bursts are equal to  $0.0011, 0.0012, 0.0001,$  and less than  $0.0001$ , respectively. At the same time, the significance level for the octupole of the correlations between the long BATSE and BeppoSAX bursts is equal to  $0.0325$ , and that for the quadrupole of the correlation map between the long BATSE bursts and CMB fluctuations is equal to  $0.0614$ . Figure 15 shows the map of one of the harmonics ( $\ell = 7$ ) in the distribution of the correlation coefficients between the positions of short BATSE and BeppoSAX bursts. Figure 16 shows the maps of the peak harmonics ( $\ell = 3$  for short and  $\ell = 2$  for long bursts) in the spectrum of the maps of correlations between the BATSE and CMB.

A distinguishing feature of the maps shown with superimposed coordinate grids are the positions of the poles of coordinate systems. It is evident from Fig. 15 that the ecliptic poles are located at special points—in the saddles between the maxima and minima of the signal distribution on the map. Similarly, the equatorial poles are located in the saddles in the map of the correlation octupole (the left panel in Fig. 16). We can see in the right panel (the quadrupole) of Fig. 16 that the poles are located in

the minima of the quadrupole. We use the method described above based on the generation of 10,000 random realizations of the GLESP pixelization with 102 pixels at the equator to estimate the statistical significance of such a configuration i.e., the probability for the minima of the quadrupole to occur in the 5-degree radius areas centered on the equatorial poles, and find it to be equal to  $0.0035$ .

## 5. DISCUSSION

Our analysis of correlations between the maps of GRB positions and the CMB shows that such correlations do exist. Of great interest is the orientation (phase properties) of correlation maps, where we can point out two points: (1) in the case of the correlations between the short GRB positions in different catalogs and their correlations with the CMB, the features found (the positions of the poles) are observed both in the equatorial and ecliptic coordinate systems; moreover, despite a small number of short BeppoSAX and BATSE events, the correlations between their positions in  $500' \times 500'$  windows exhibit a chain of events in the ecliptic plane (the top left panel in Fig. 12), and a predominant occurrence of the correlated pixels in the Southern Hemisphere; (2) the correlations between the long BATSE events and CMB fluctuations exhibit features in the equatorial coordinate system,

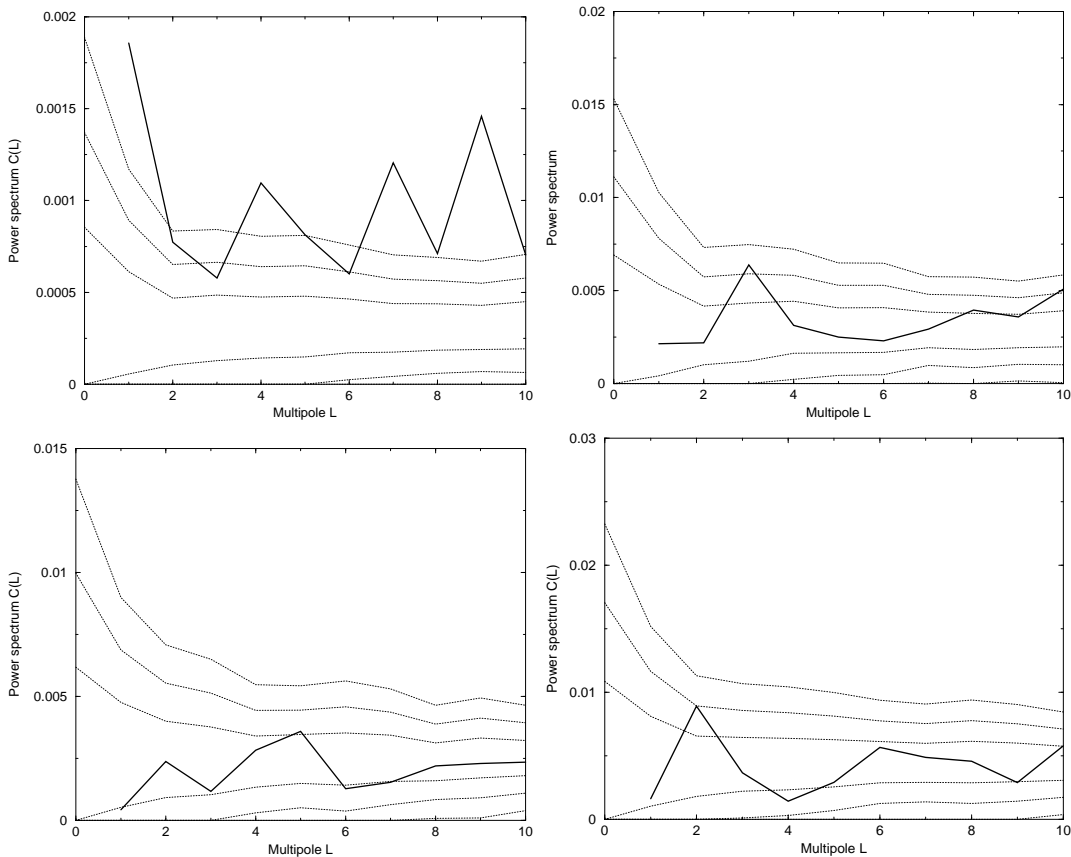


Figure 13: *Power spectra of the correlation coefficient maps between the BATSE GRB positions and BeppoSAX and CMB data ( $\ell_{max} = 26$ ) (the solid line). The pixel size of the correlations is  $500' \times 500'$ . The top left panel shows the spectrum of correlation between the BATSE and BeppoSAX data,  $t < 2$  s. The top right panel shows the spectrum of correlation between the BATSE ( $t < 2$  s) and CMB data. The bottom left panel shows the spectrum of correlation between the BATSE and BeppoSAX data,  $t > 2$  s. The bottom right panel shows the spectrum of correlation between the BATSE ( $t > 2$  s) and CMB data. The dashed lines show the  $\pm\sigma$ ,  $\pm 2\sigma$ , and  $\pm 3\sigma$  deviations from the mean, where  $\sigma$  is estimated from the spectra of 200 simulated random realizations of the zero hypothesis, which assumes a uniform distribution of gamma-ray bursts in the sky and the Gaussian CMB amplitude distribution corresponding to the  $\Lambda$ CDM cosmology.*

while the joint probability of high quadrupole amplitude and of the quadrupole minimum occurrence at the equatorial pole is practically equal to zero in the case of correlation with random maps.

The correlations found between the GRB positions and the CMB, that are sensitive to the equatorial coordinate system must be due to the systematic effects. This way, a relatively greater number of gamma-ray events near the equatorial poles may be due to longer exposures of the satellite cameras due to the observing method employed. Both satellites that observed the gamma-ray bursts moved in rather low Earth orbits, rendering the areas located near the celestial equator periodically unobservable. At the same time, for the CMB data such a sensitivity to the equatorial coordinate system is impossible

to explain in terms of such a simple model, as the microwave background data were obtained onboard the WMAP satellite, which rotates about the L2 Lagrangian point. Note that in our previous paper [11] we also found some correlations to be “aware” of the equatorial system. We do not rule out the possible contribution from the Earth’s magnetic field, which has a large extent and shows up as large-scale correlations of the microwave background. However, we do not understand the mechanism of such correlations.

Neither do we understand the possible interrelation between the ecliptic plane and the positions of gamma-ray bursts. Here the situation is reversed: the ecliptic features in the CMB data have already been discussed recently [12, 13, 11], however, further studies are needed to understand what may link gamma-

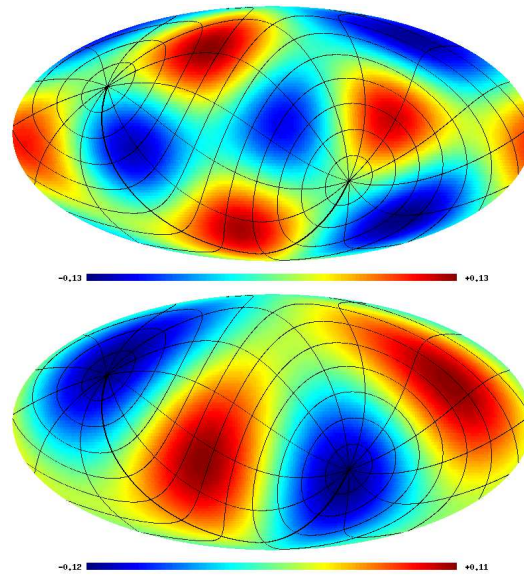


Figure 16: Maps of the harmonics identified in the power spectrum (Fig. 13). Correlation maps between the BATSE burst positions ( $t > 2$  s) and the BeppoSAX data (the top panel,  $\ell = 3$ ) and between the BATSE burst positions ( $t > 2$  s) and the CMB (the bottom panel,  $\ell = 2$ ) with the equatorial coordinate grid superimposed.

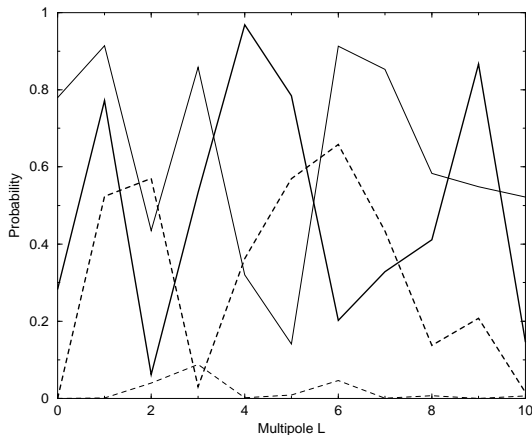


Figure 14: Significance levels for the deviations from the mean level for the power spectra of the correlation maps: short gamma-ray burst BATSE-BeppoSAX correlations (the thin dashed line); long gamma-ray burst BATSE-BeppoSAX correlations (the thick dashed line); short BATSE bursts and CMB fluctuations (the thin solid line), and long BATSE bursts and CMB fluctuations (the thick solid line). The statistical significance was estimated via direct numerical simulations involving 10000 random realizations of the zero hypothesis, which consists in the uniform GRB distribution in the sky and the Gaussian CMB amplitude distribution corresponding to the  $\Lambda$ CDM cosmology.

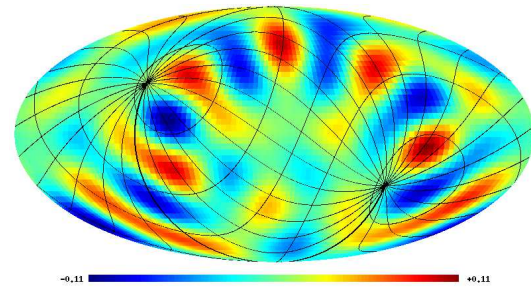


Figure 15: Map of the seventh harmonic ( $\ell = 7$ ) in the expansion of the map of correlations between the positions of short BATSE and BeppoSAX bursts with the equatorial coordinate grid superimposed.

ray evens and the ecliptic plane. One of the possible hypotheses explains this feature as a selection effect due to the fact that the observing instruments of the satellites are turned away from the Sun, and this may put the plane of the ecliptic in a special position.

Note also that the correlation properties of the CMB, which show up in the “near-Earth” coordinate systems when the data with “randomly” distributed events are used, are indicative of the non-Gaussian nature of the data for low-order multipoles, which may be due either to the systematic effects, or to a hitherto unexplored effect in the near-Earth space. We consider further studies of this correlation to be of especially great interest given that the new high-quality data are expected to be provided by the Fermi

and Planck missions.

**Acknowledgments.** We are grateful to Valery Larionov (St. Petersburg State University) for useful discussions of the results of this work. We thank the NASA for making available the NASA Legacy Archive, from where we adopted the WMAP data. We are also grateful to the authors of the HEALPix<sup>4</sup> [14] package, which we used to transform the WMAP7 maps into the coefficients  $a_{\ell m}$ . This work made use of the GLESP<sup>5</sup> [15, 16] package for the further analysis of the CMB data on the sphere. This work was supported by the Program for the Support of Leading Scientific Schools of Russia (the School of S. E. Khaikin) and the Russian Foundation for Basic Research (grant nos. 09-02-00298 and 08-02-00486. O.V.V. also acknowledges partial support from the Foundation for the Support of Domestic Science (the program “Young Doctors of Science of the Russian Academy of Sciences”) and the Dynasty Foundation.

## References

- D. Riccia, F. Fioreb, and P. Giommia, Nuclear Physics B - Proc. Suppl. **69**, 618 (1999).
- W. S. Paciasas, C. A. Meegan, G. N. Pendleton, et al. Astrophys. J. Supp. **122**, 465 (1999), astro-ph/9903205.
- L. L. R. Williams and N. Frey, Astrophys. J. **583**, 594 (2003).
- A. Mészáros, L. G. Balázs, Z. Bagoly, and P. Veres, arXiv:0906.4034
- Ya. B. Zeldovich and R. A. Sunyaev. Astrophys. Space Sci. **4**, 301 (1969).
- R. K. Sachs and A. M. Wolfe, Astrophys. J. **147**, 73 (1967).
- N. Jarosik, C. L. Bennett, J. Dunkley, et al., Astrophys. J. Supp., submitted (2010), arXiv:1001.4744.
- C. L. Bennett, M. Halpern, G. Hinshaw, et al., Astrophys. J. Supp. **148**, 1 (2003), astro-ph/0302207.
- O. V. Verkhodanov, M. L. Khabibullina, and E. K. Majorova, Astrophys. Bull. **64**, 263 (2009).
- A. G. Doroshkevich, O. B. Verkhodanov, O. P. Naselsky, et al., arXiv0904.2517 (2009).
- O. V. Verkhodanov and M. L. Khabibullina, Astrophys. Bull. **65**, accepted (2010).
- J. M. Diego, M. Cruz, J. Gonzalez-Nuevo, et al., arXiv:0901.4344 (2009).
- V. Dikarev, O. Preuss, S. Solanki, et al., Astrophys. J. **705**, 670 (2009).
- K. Górski, E. Hivon, A. J. Banday, et al., Astrophys. J. **622**, 759 (2005).
- A. G. Doroshkevich, P. D. Naselsky, O. V. Verkhodanov, et al., Int. J. Mod. Phys. D **14**, 275 (2003), astro-ph/0305537.
- O. V. Verkhodanov, A. G. Doroshkevich, P. D. Naselsky, et al., Bull. Spec. Astrophys. Obs. **58**, 40 (2005).

---

<sup>4</sup> <http://www.eso.org/science/healpix/>